Effect of Surface Energy on Size-Dependent Deformation Twinning of Defect-Free Au Nanowires

Byungil Hwang‡[1], Mijeong Kang‡[2], Subin Lee[3], Christopher R. Weinberger[4], Phillip Loya[5],

Jun Lou[5], Sang Ho Oh[3], Bongsoo Kim*[2], and Seung Min Han*[1].

1. Graduate School of Energy Environment Water and Sustainability, Korea Advanced

Institute of Science & Technology, Daejeon, Republic of Korea, 305-701

2. Department of Chemistry, Korea Advanced Institute of Science & Technology, Daejeon,

Republic of Korea, 305-701

3. Department of Materials Science and Engineering, Pohang University of Science and

Technology (POSTECH), Pohang, Republic of Korea, 790-784

4. Department of Mechanical Engineering and Mechanics, Drexel University, Philadelphia,

USA, PA 19104

5. Department of Materials Science and Nano Engineering, Rice University, Houston, USA,

TX 77005.

In this study, we report the size-dependent transition of deformation twinning studied using

in-situ SEM/TEM tensile testing of defect-free [110] Au nanowires/ribbons with controlled

geometry. The critical dimension below which the ordinary plasticity transits to deformation

twinning is experimentally determined to be ~170 nm for Au nanowires with equilateral

cross-sections. Nanoribbons with fixed thickness but increased width-to-thickness ratios (9:1)

were also studied to show that an increase in the surface energy due to the crystal re-

orientation suppresses the deformation twinning. Molecular dynamics simulations confirmed that the transition from partial dislocation mediated plasticity to perfect dislocation plasticity with increase in the width-to-thickness ratio is due to the effect of the surface energy.

1. Introduction

Plasticity of defect-free metal nanowires is known to be uniquely different from that of bulk counterparts in that there is a lack of pre-existing dislocations and, therefore, plasticity occurs through the nucleation of new dislocations from the surface, which requires high stresses that approach the theoretical strength of metal.[1-8] Furthermore, dislocation interactions and multiplications that are typically observed in bulk metals are severely limited in metal nanowires since the nucleated dislocations can easily annihilate at free surfaces.[9-16, 36-39] Several previous studies reported ultra high strength in metal nanowires that approach the theoretical strength as a result of the difficulty in nucleation and multiplication of dislocations within the nanoscale volume of metal nanowires.[17-21]

In the absence of pre-existing dislocations, which are needed for plastic deformation, deformation twinning becomes a competitive process.[17, 22-27] In face centered cubic (FCC) metals, deformation twinning involves the sequential nucleation of partial dislocations that causes an orientation change in the deformed volume via the formation of a twin. In the case of the bulk FCC metals, deformation twinning typically occurs at high strain rates or at low temperatures.[28] However, it has been well established that deformation twinning is an important deformation mechanism in nanocrystalline metals. For example, Chen et al. reported that the twin deformation can occur in nanocrystalline Al even at ambient temperatures and moderate strain rates if the grain size is below a critical length scale.[22] In their study, Chen et al. postulated that the size dependent nucleation stress of perfect vs. partial dislocations govern the transition from dislocation plasticity to deformation twinning.

The competition arises since the partial dislocations, which represent twin embryos, have smaller Burgers vectors than perfect dislocations, but the formation of stacking faults for nucleation of a partial dislocation costs additional energy in comparison to nucleation of perfect dislocations that do not form stacking faults. Therefore, the stress required to nucleate a partial dislocation (τ_P) and a perfect dislocation (τ_N) are given by

$$\tau_P = \frac{2\alpha\mu b_p}{D} + \frac{\gamma_{SF}}{b_p} \ (1), \qquad \tau_N = \frac{2\alpha\mu b_N}{D} \ (2),$$

where μ is the shear modulus, γ_{SF} is the stacking fault energy, and b_P is the magnitude of the Burgers vectors for leading partial dislocation. α is 0.5 and 1.5 for edge and screw dislocations, respectively. By equating equations (1) and (2), a simple analytical model[22] for the critical diameter below which twin deformation dominates can be defined as

$$D_c = \frac{2\alpha\mu(b_N - b_p)b_p}{\gamma_{SF}} \ (3).$$

Therefore, Eq. (3) predicts a size-dependent transition from ordinary plasticity via propagation of perfect dislocations to partial dislocation mediated plasticity or deformation twinning. This critical dimension was later modified by Sedlmayr et al.[20] to consider the contribution from different Schmid factors for full and partial dislocations as discussed further in the Supporting Information 01. Although theoretically predicted, there is a lack of definitive experimental results that verify the length scale for this transition from ordinary dislocation slip to deformation twinning.

Deformation twinning was also observed for [110] oriented Au nanowires with a diameter of ~150 nm in the *in-situ* SEM study by Seo et al., who reported that these nanowires can deform via twin propagation resulting in strains as large as 41%, thus referring to this as "superplastic" behavior.[5] In a [110] oriented Au nanowire, the initial nucleation of leading partial dislocation ($b=a/6\langle11\bar{2}\rangle$) is subsequently followed by another leading partial dislocation of the same Burgers vector on an adjacent crystallographic plane resulting in the formation of an embryonic twin band, which is then extended coherently along the length of

the nanowire. As a result of this deformation twinning, the deformed section of the nanowire re-orients from {111} to {100}, and accordingly, the free surfaces also re-orient from {111} to {100} planes with different surface energies as illustrated in Fig. 1. Therefore, an interesting question arises as to what the role of the change in surface energy will have on the overall deformation of the Au nanowires. The role of the surface area is expected to be especially important for these nanowires with high surface area to volume ratios.

Here, we attempt to address the following two important factors that govern the deformation behavior in gold nanowires: the length scales for the transition from ordinary dislocation plasticity to deformation twinning and the role of the surface energies in controlling deformation twinning. In this study, the critical dimension of [110] Au nanowires with equilateral area is experimentally determined using *in-situ* SEM/TEM tensile tests using push-to-pull (PTP) devices developed by Ganesan et al.[29] After determining the critical dimension below which deformation twinning occurs in the [110] Au nanowires, the thickness of the nanowire was fixed below this critical dimension and the width of the nanowire was systematically varied to study the effect of the surface area on the deformation mechanisms in these nanowires. In addition to the direct observations of the deformation behavior using *in-situ* SEM as well as *in-situ* TEM (for specific samples), MD simulations were also performed to confirm the effect of surface energy on deformation twinning of the Au nanoribbons.

2. Results and discussion

2.1. Size-dependent deformation twinning in defect-free [110] Au nanowires.

In order to study the size-dependent deformation behavior, defect-free [110] Au nanowires with diameters ranging from 75 nm to 392 nm were first tested in tension and the SEM images of the deformed nanowires are shown in Fig. 2. The SEM images revealed a clear transition in the deformation behavior as diameter of the nanowire was increased. Au

nanowires with diameter less than 167 nm deformed via deformation twinning through length of the nanowire, and therefore, showed "superplastic" behavior that was also observed by Seo et al.[5] (see Supporting Movie 01). On the other hand, localized deformation or necking was observed followed by sudden failure in the nanowires with diameters larger than 167 nm (see Supporting Movie 02). This clear transition from ordinary plasticity to "superplastic" deformation twinning occurred at the critical dimension of $D_c \sim 170$ nm.

Several evidences confirmed that the deformation in the nanowires with diameters smaller than ~170 nm indeed proceeded via deformation twinning. Twinning is known to cause crystallographic re-orientation in [110] Au nanowires having a rhombic cross section with {111} side facets to [100] axial orientation with {100} side facets.[21] SEM images of the deformed section of the nanowires with diameters smaller than ~170 nm indicated a tilt angle of ~18.0°, which is consistent with the expected misorientation angle between the twinned and the non-twinned sections of the [110] Au nanowire,[25] as shown in Fig. 2a-d. The selected area diffraction (SAD) pattern shown in Fig. S2a-c also confirmed that the twinned region of the deformed Au nanowire with diameter of 102 nm has [100] orientation while the untwined region remains in its original [110] orientation (see Supporting Information 02).

While clear deformation twinning was observed in nanowires with diameters smaller than D_c, nanowires with larger diameters exhibited contrasting deformation behavior. *In-situ* TEM observations with snapshots shown in Fig. 3a-e revealed that nanowires with a diameter of 620 nm deformed by formation of localized neck upon onset of plasticity that resulted in tensile failure. Multiple slip traces were observed in the plastically deformed region of the nanowires as shown in Fig. 3f, and the angle between the slip trace and the nanowire axis was measured to be ~30.0°, which is in agreement with the expected angle for {111} slip plane. The observation of necking together with the presence of slip traces that indicate activation of multiple slip systems is indicative of ordinary plasticity that is similar to the well-known tensile deformation of bulk metals. The cause for this clear transition from deformation

twinning to ordinary plasticity for nanowires with diameter larger than D_c can be explained by the fact that the energy cost associated with the stacking fault becomes larger than the stresses needed to nucleate a full dislocation as the nanowire diameter is increased, as proposed by Chen et al.[22]

The stress-strain behavior of two nanowires with diameters of 102 nm and 392 nm are shown in Fig. 4 encompassing both deformation twinning and ordinary plasticity. The nanowire with diameter of a 102 nm that deformed via twinning exhibited ductility of 39.7%, which is close to the theoretical calculation based on orientation change. Upon passing the elastic limit at 3.6%, plasticity starts at 1.63 GPa, which is close to the theoretical strength of Au (1.8 GPa),[30] followed by a sudden drop in stress due to the onset of twin propagations that results in plasticity at significantly lower stress. The high strength is due to the high stress needed to nucleate the leading partial dislocation from the surface of the defect-free Au nanowire, while the stress drop after the onset of twin propagation is due to the easier subsequent nucleations of partial dislocations on adjacent planes due to local stress concentrations at the slip step.[20]

The nanowires with diameters larger than D_c elastically deformed with a yield strength of 1.55 GPa, which is also close to the theoretical strength, similar to the stress where twin propagation started in the nanowires with diameters smaller than D_c. However, instead of exhibiting "superplasticity" or deformation twinning, nanowires with diameters larger than D_c resulted in sudden failure shortly after the onset of plasticity above the elastic limit of 4.6%. In the absence of pre-existing dislocations, the first step in plasticity for all our nanowires, regardless of the ultimate deformation mechanism, is the nucleation of a leading partial dislocation. This is supported by the observation that the nucleation stresses for nanowires of different sizes is the same, regardless of whether they deform via twinning or perfect dislocations. Thus, the incipient plastic event must be the same: the nucleation of a leading partial dislocation. The difference between ordinary plasticity and deformation twinning can,

therefore, be attributed to the competition between the nucleation of a trailing partial vs. another leading partial on an adjacent slip plane, and the former results in localized deformation via neck formation that causes limited ductility whereas the later results in twin deformation by continued nucleation of leading partials. There is small degree of non-linearly during the initial loading segment of the stress-strain curves in Fig. 4, and this is expected to be due to small degree of slip or settling-in of the grips or any mis-alignment. However, the loading slope is 68 GPa, which is close to the expected modulus of Au (78 GPa).

2.2. Deformation behavior of defect-free Au nanoribbons.

As explained above, the deformation twinning re-orients the nanowire surface from {111} to {100}, and this is expected to contribute to suppression of the deformation twinning. To experimentally investigate the role of surface energy in controlling deformation twinning, nanoribbons with thickness fixed below D_c (i.e. in the range for preferential twin deformation) and increased widths from 122 nm to 1109 nm, which corresponds to width-to-thickness ratio of 1:1 and 9:1, were investigated. Interestingly, despite having a similar thickness to that of the Au nanowire that showed deformation twinning, the twin propagation was not observed in nanoribbons with large width-to-thickness ratio of 9:1. The fractured surface of the nanoribbon shown in Fig. 5a indicates that the failure of the nanoribbons occurred by activation of two different slip systems that resulted in deformation. Furthermore, SAD analysis confirmed that the nanoribbons retained their [110] orientation after failure, as shown in Fig. 5b-d. The deformation of nanoribbons, which has large width-to-thickness ratio, is similar to the deformation of a sheet metal in that necking only occurs in the thickness direction without large contraction in the width upon application of uniaxial tensile load.[31] The stress-strain curve of the nanoribbon, as shown in Fig. 5e, indicates brittle failure of the nanoribbon with no ductility after yield, which is in direct contrast to the "superplastic" or deformation twinning observed in nanowires with the same diameter. The strength of the

nanoribbon was 1.50 GPa, which is similar to that of the nanowires, 1.55 GPa, and again indicates that the initial plastic event is the same: the nucleation of a leading partial dislocation and the differences lie in the nucleation of subsequent leading or trailing partial dislocations.

The transition from deformation twinning to ordinary dislocation plasticity for nanoribbons with increased widths can be understood again in terms of the competition between the energy cost associated with stacking faults and partial Burgers vectors in leading partial dislocations and the formation of full Burgers vectors in perfect dislocations. In addition, the deformation twinning causes the {111} side surfaces to be re-oriented to {100} surfaces with higher surface energy (γ_{111} =1.52 Jm^{-2} and γ_{100} = 1.80 Jm^{-2}),[32] which increases the energy barrier for twin deformation. Therefore, the larger surface area of the nanoribbons is expected to deform via perfect dislocations in contrast to nanowires with equilateral cross-sectional areas that deformed via twinning.

To further confirm the influence of surface area on the observed transition from deformation twinning to ordinary dislocation plasticity in Au nanoribbons with varying width-to-thickness ratios, we performed MD simulations of nanoribbons. The thickness of the nanoribbons were held at 5 nm and the width was varied from 5 nm to 50 nm and the length that was 5 times the width. Additional simulation details are listed in Supporting Information 03. In all cases, the sizes of these nanowires are well below the critical dimension identified in the experiments. Fig. 6 provides snapshots of the MD simulation results for tensile testing of nanoribbons with two widths, 5 nm and 50 nm. In the nanowire with equilateral cross-sections, deformation twinning is the dominant plastic process, resulting in the re-orientation of the nanowire (Fig. 6a, b), in agreement with previous MD simulations.[20, 24-26] As the width increases, the deformation transitions from twin dominated deformation to ordinary dislocation plasticity (Fig. 6c-f). The simulations not only qualitatively agree with the experiments, but allow for systematic identification of the key reasons for such a transition.

First, partial dislocations are always nucleated first, regardless of the aspect ratio of the nanoribbon and in all simulations, very small nanotwins are observed. However, as deformation continues, trailing partial dislocations are nucleated on the same plane as the leading, creating perfect dislocations. This deformation occurs such that the trailing partial dislocations remove the surface steps on the large surface areas of the nanowire, ultimately leaving surface traces only on the {111} free surfaces with a small surface area. The reduction in energy by the removal of surface steps drives deformation to perfect dislocations. However, the simulations tend to over predict the ductility of the nanoribbons, which can be attributed to the short length of the nanowires used (and potentially strain rate), as pointed out in a recent study.[33] Thus, the elimination of surface steps drives the energetics of partial dislocation to prefer trailing partials, and thus perfect dislocations, over twinning dislocations.

Based on our experimental and MD simulation observations that increased surface energy associated with the re-orientated section of the nanoribbons can result in change in the critical length scale for deformation twinning, we propose the revised model for the nucleation stress of full dislocation and partial dislocation from the work by Chen et al. (Eq 1).[22] The equation for the nucleation stress of the partial dislocation that accounts for the surface re-orientation, therefore, can be obtained by adding an additional term associated with the stress needed to overcome the energy cost arising from the difference in surface energies:

$$\tau_{P'} = \frac{2\alpha\mu b_p}{D} + \frac{\gamma_{SF}}{b_p} + \frac{\Delta S}{D} \ (4)$$

where D is the diameter of the nanowire, ΔS is the additional term associated with the differences in surface energies as well as the surface areas upon re-orientation that is given by $\Delta S = \left[4\sqrt{3}\left(\gamma_{100} - \frac{\sqrt{3}}{2}\gamma_{111}\right)\right]/(\sqrt{2}-1)$, and γ_{100} and γ_{111} are the surface energies for {100} and {111} surfaces, respectively. The expression for ΔS was taken from the work by Seo et al.[6] and is explained in the Supporting Information 04. Equating the above equation to the

9

nucleation stress of a full dislocation given by Eq 2, a revised analytical model for the critical dimension for the transition can be written as

$$D_{c'} = \frac{2\alpha\mu(b_N - b_p)b_p - \Delta S \cdot b_p}{\gamma_{SF}} \quad (6)$$

Using the above relation, the critical dimension for Au nanowire was calculated to be 33 nm, which is 10% larger than the value from the previous model by Chen et al., 30 nm. Therefore, this revised model is able to explain the trend of increase in D_c by accounting for the cost in energy associated with increase in surface energy of twinned sections. It should be noted, however, that this model is a lower limit and there exists still a notable difference between experimental and calculated values of critical dimensions using this model. The first reason for the difference is that the nucleation in the experiments may not occur between the two furthest pinning points that span across the diameter, but is likely to be nucleated from a smaller distance. Therefore, the experimental nanowire dimension has to be larger than what is predicted from the model calculations. In addition, this model does not account for stress concentration that favors nucleation of another leading partial dislocation once the leading partial dislocation produces a slip step on the surface. The presence of stress concentrations would result in an increase in the critical dimension for the transition from deformation twinning to ordinary dislocation plasticity.

3. Experimental Section

Synthesizing defect-free Au nanowires and nanoribbons: Single-crystalline Au nanowires and nanoribbons were synthesized on a sapphire substrate in a horizontal quartz tube furnace by using previously described vapor transport method.[34] A Au slug was placed in the middle of a heating zone and sapphire substrates were put a few centimeters downstream from the Au slug. While maintaining a chamber pressure of ~5 Torr with the flow of Ar gas at a rate of 100 standard cubic centimeter per minute, the Au slug was heated up to ~ 1130 °C.

Au nanowires and nanoribbons were subsequently grown on the substrate for ~30 min of

reaction time. Their width and length were adjusted by controlling synthetic parameters such

as heating temperature. The synthesized Au nanowires and nanoribbons showed defect-free

fcc crystalline structure as shown in the SAD patterns observed at different zone axes (Fig.

S5). All diffraction spots can be assigned to the fcc Au crystal and no additional spots

indicating defects or twins were observed. The dimensions of the nanowires were measured

by using SEM as described further in Supporting Information 06.

In-situ tensile tests: A tungsten probe tip was used to pick-up the Au

nanowires/ribbons that were vertically grown on the sapphire substrate. In order to perform

tensile tests, an individual Au nanowire/ribbon was then placed on the PTP device that was

specifically designed to perform nanoscale tensile tests (see Supporting Information 07).[29, 35]

Once the Au nanowire/ribbon was properly placed on the PTP device, tensile tests were

performed inside a SEM (Quanta 3D FEG) equipped with a Picoindentor (PI85, Hysitron

Co.,) under constant displacement rate of 15 nm/sec until failure. The stress vs. strain curves

of the nanowires/ribbons were determined from recorded load-displacement data as described

in the Supporting Information 08. For *in-situ* TEM tests, a nanoindentation TEM holder

(Nanofactory) with a diamond flat punch tip was used in a TEM operated at 200 kV (JEM-

2100F, JEOL) equipped with a charge coupled device camera (ORIUS 200D, Gatan) that was

used to acquire real-time videos.

4. Conclusion

In conclusion, we have experimentally determined the critical dimension for the

transition from ordinary dislocation plasticity to deformation twinning in Au nanowires to be

~170 nm via *in-situ* SEM/TEM analysis. In addition to this size dependent transition, Au

nanoribbons with increased width-to-thickness ratio of 9:1 were studied to understand the

effect of surface area, and hence surface energy, on the deformation mechanism in these nanowires. Deformation twinning was not observed for the case of nanoribbons with large width-to-thickness-ratio of 9:1 even when the thickness was below D_c. This transition is attributed to the increase in surface energy associated with re-orienting the {111} sides surfaces to {100} in the twinned section of the nanoribbon. The role of surface area in controlling deformation was confirmed through MD simulations that showed a similar trend in transition from twinning to perfect dislocation plasticity for large width-to-thickness ratio nanoribbons. Lastly, a revised model for critical dimension for transition in deformation mechanism was proposed that accounts for the difference in surface energy of twinned section of the nanowire.

Corresponding Author

*E-mail: smhan01@kaist.ac.kr, bongsoo@kaist.ac.kr

Author Contributions

‡B.I Hwang and M.J. Kang contributed equally to this work.

Nanoscale Accepted Manuscript

1.   Y. Lu, J. Song, J. Huang and J. Lou, *Nano Res.*, 2011, **4**, 1261-1267.

2.   Y. Lu, J. Song, J. Y. Huang and J. Lou, *Adv. Funct. Mater*, 2011, **21**, 3982-3989.

3.   C. Peng, Y. Ganesan, Y. Lu and J. Lou, *J. Appl. Phys.*, 2012, **111**, 063524.

4.   G. Richter, K. Hillerich, D. S. Gianola, R. Monig, O. Kraft and C. A. Volkert, *Nano Lett.*, 2009, **9**, 3048-3052.

5.   J. H. Seo, Y. Yoo, N. Y. Park, S. W. Yoon, H. Lee, S. Han, S. W. Lee, T. Y. Seong, S. C. Lee, K. B. Lee, P. R. Cha, H. S. Park, B. Kim and J. P. Ahn, *Nano Lett.*, 2011, **11**, 3499-3502.

6.   J. H. Seo, H. S. Park, Y. Yoo, T. Y. Seong, J. Li, J. P. Ahn, B. Kim and I. S. Choi, *Nano Lett.*, 2013, **13**, 5112-5116.

7.   B. Wu, A. Heidelberg and J. J. Boland, *Nat. Mater.*, 2005, **4**, 525-529.

8.   Y. Zhu, Q. Qin, F. Xu, F. Fan, Y. Ding, T. Zhang, B. J. Wiley and Z. L. Wang, *Phys. Rev. B.*, 2012, **85**.

9.   J. R. Greer and W. D. Nix, *Phys. Rev. B.*, 2006, **73**.

10.   J. R. Greer, W. C. Oliver and W. D. Nix, *Acta Mater.*, 2005, **53**, 1821-1830.

11.   B. Hwang, H.-A. S. Shin, T. Kim, Y.-C. Joo and S. M. Han, *Small*, 2014, **10**, 3397-3404.

12.   D. Jang and J. R. Greer, *Scripta Mater.*, 2011, **64**, 77-80.

13.   D. Jang, X. Li, H. Gao and J. R. Greer, *Nat. Nanotechnol.*, 2012, **7**, 594-601.

14.   D. Kiener, P. Hosemann, S. A. Maloy and A. M. Minor, *Nat. Mater.*, 2011, **10**, 608-613.

15.   D. Kiener and A. M. Minor, *Nano Lett.*, 2011, **11**, 3816-3820.

16.   S. H. Oh, M. Legros, D. Kiener and G. Dehm, *Nat. Mater.*, 2009, **8**, 95-100.

17.   S. Lee, J. Im, Y. Yoo, E. Bitzek, D. Kiener, G. Richter, B. Kim and S. H. Oh, *Nat. Commun.*, 2014, **5**, 3033.

18.   S. H. Oh, M. Legros, D. Kiener, P. Gruber and G. Dehm, *Acta. Mater.*, 2007, **55**, 5558-5571.

19.   C. Peng, Y. Zhan and J. Lou, *Small*, 2012, **8**, 1889-1894.

20.   A. Sedlmayr, E. Bitzek, D. S. Gianola, G. Richter, R. Mönig and O. Kraft, *Acta. Mater.*, 2012, **60**, 3985-3993.

21.   C. R. Weinberger, A. T. Jennings, K. Kang and J. R. Greer, *J. Mech. Phys. Solids.*, 2012, **60**, 84-103.

22.   M. Chen, E. Ma, K. J. Hemker, H. Sheng, Y. Wang and X. Cheng, *Science*, 2003, **300**, 1275-1277.

23.   C. Ji and H. S. Park, *Appl. Phys. Lett.*, 2006, **89**, 181916.

24.   H. S. Park, K. Gall and J. A. Zimmerman, *J. Mech. Phys. Solids.*, 2006, **54**, 1862-1881.

25.   E. Bitzek, *J. Sol. Mech. Mater. Eng.*, 2012, **6**, 99-105.

26.   C. R. Weinberger and W. Cai, *J. Mater. Chem.*, 2012, **22**, 3277.

27.   Y. Yue, P. Liu, Q. Deng, E. Ma, Z. Zhang and X. Han, *Nano Lett.*, 2012, **12**, 4045-4049.

28.   M. A. Meyers, O. Vöhringer and V. A. Lubarda, *Acta Mater.*, 2001, **49**, 4025-4039.

29.   Y. Ganesan, L. Yang, P. Cheng, L. Hao, R. Ballarini and L. Jun, *J. Microelectromech. Syst.*, 2010, **19**, 675-682.

30.   S. Ogata, J. Li, N. Hirosaki, Y. Shibutani and S. Yip, *Phys. Rev. B.*, 2004, **70**.

31.   R. Schneider, B. Heine, R. Grant and Z. Zouaoui, *Proceedings of the Institution of Mechanical Engineers, Part L: Journal of Materials Design and Applications*, 2015, **229**, 126-136.

32.   T. Fujita, P. Guan, K. McKenna, X. Lang, A. Hirata, L. Zhang, T. Tokunaga, S. Arai, Y. Yamamoto, N. Tanaka, Y. Ishikawa, N. Asao, Y. Yamamoto, J. Erlebacher and M. Chen, *Nat. Mater.*, 2012, **11**, 775-780.

33.   Z. Wu, Y.-W. Zhang, M. H. Jhon, H. Gao and D. J. Srolovitz, *Nano Lett.*, 2012, **12**,
       910-914.

34.   Y. Yoo, K. Seo, S. Han, K. S. Varadwaj, H. Y. Kim, J. H. Ryu, H. M. Lee, J. P. Ahn,
       H. Ihee and B. Kim, *Nano Lett.*, 2010, **10**, 432-438.

35.   Y. Lu, C. Peng, Y. Ganesan, J. Y. Huang and J. Lou, *Nanotechnology*, 2011, **22**,
       355702.

36.   Q. Qin, S. Yin, G. Cheng, X. Li, T.-H. Chang, G. Richter, Y. Zhu and H. Gao, *Nat.
       Commun.*, 2015, **6**.

37.   S. Narayanan, G. Cheng, Z. Zeng, Y. Zhu and T. Zhu, *Nano Lett.*, 2015, **15**, 4037-
       4044.

38.   R. A. Bernal, A. Aghaei, S. Lee, S. Ryu, K. Sohn, J. Huang, W. Cai and H. Espinosa,
       Nano Lett., 2015, **15**, 139-146.

39.   T. Filleter, S. Ryu, K. Kang, J. Yin, R. A. Bernal, K. Sohn, S. Li, J. Huang, W. Cai
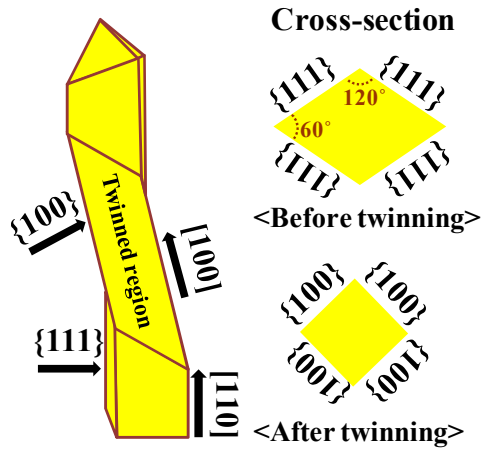   and H. D. Espinosa, *Small*, 2012, **8**, 2986-2993.

Fig. 1 A schematic of a Au nanowire deformed by twinning illustrating its cross-section before and after deformation twinning. The [110] oriented Au nanowire initially has a rhombic cross-section with {111} free surfaces, but changes to a rectangular cross-section with {100} free surfaces after twinning.
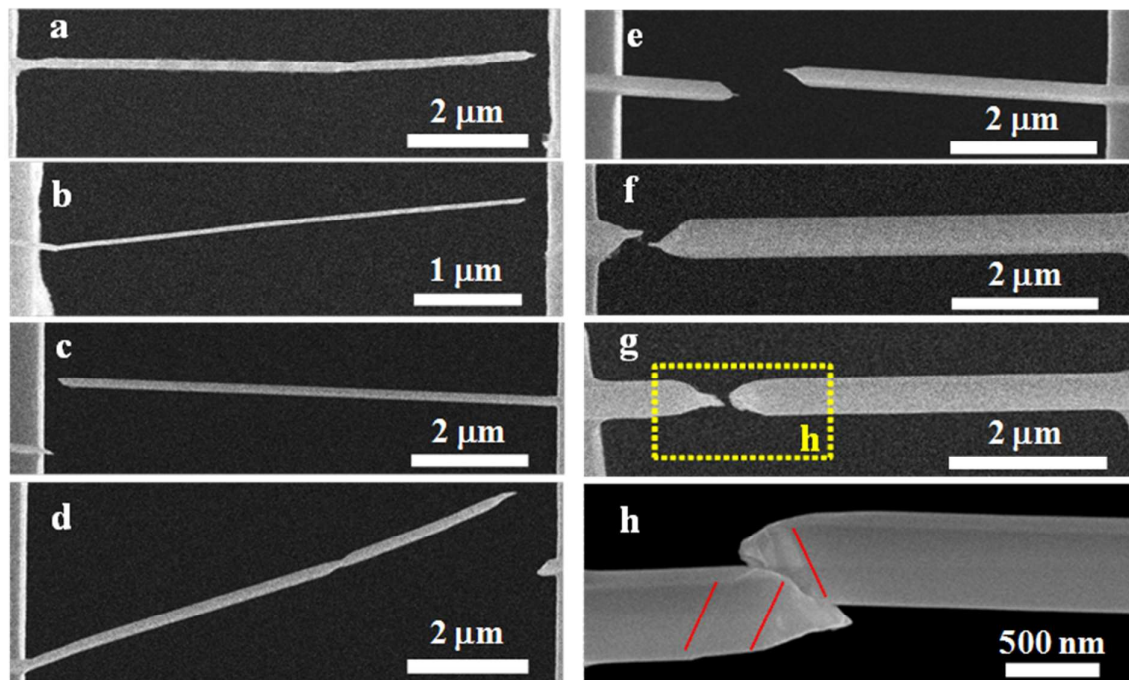
Fig. 2 SEM images of defect-free [110] oriented Au nanowires after testing to failure under tension. Nanowires with diameter of (a) 75 nm, (b) 102 nm, (c) 123 nm, (d) 132 nm showed deformation twinning while nanowires with diameter of (e) 167 nm, (f) 380 nm, and (g) 392 nm showed ordinary plasticity. (g-h) Close-up view of necking as a result of ordinary plasticity in larger nanowires.
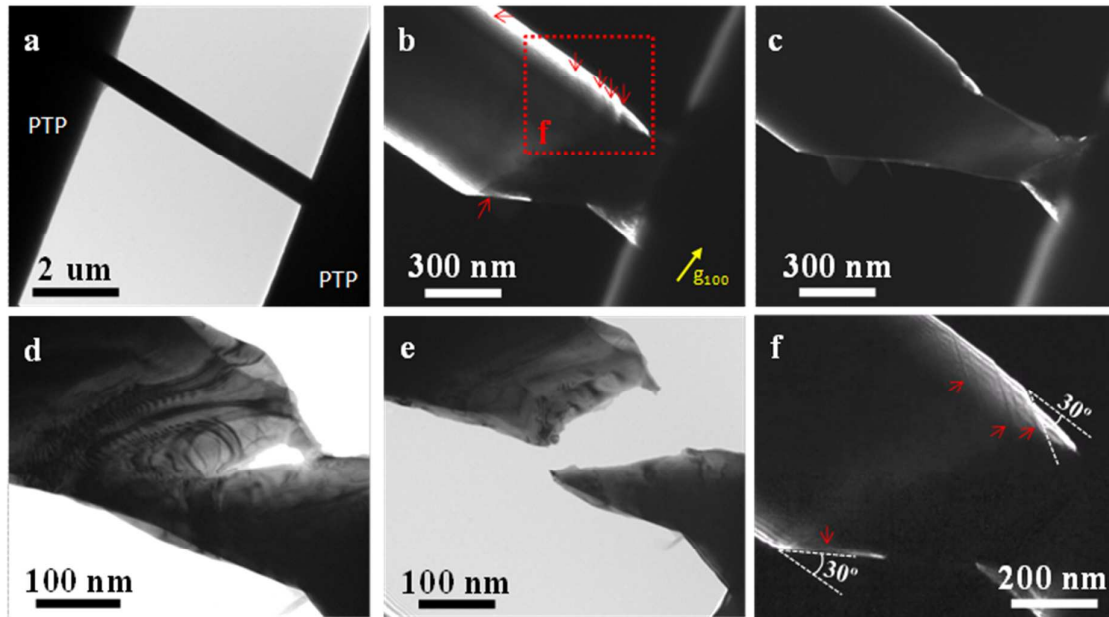
Fig. 3 TEM images of a 620 nm Au nanowire during tensile loading. (a) Initially, the Au nanowire deformed elastically, and then (b) necking occurred within the length of nanowire as the tensile strain was further increased. Multiple slip traces were observed in the necking region as further confirmed in (f), which was magnified from red square in (b). (c-e) With increasing tensile strain, plastic deformation was concentrated on the necked region, thereby resulting in observed failure.
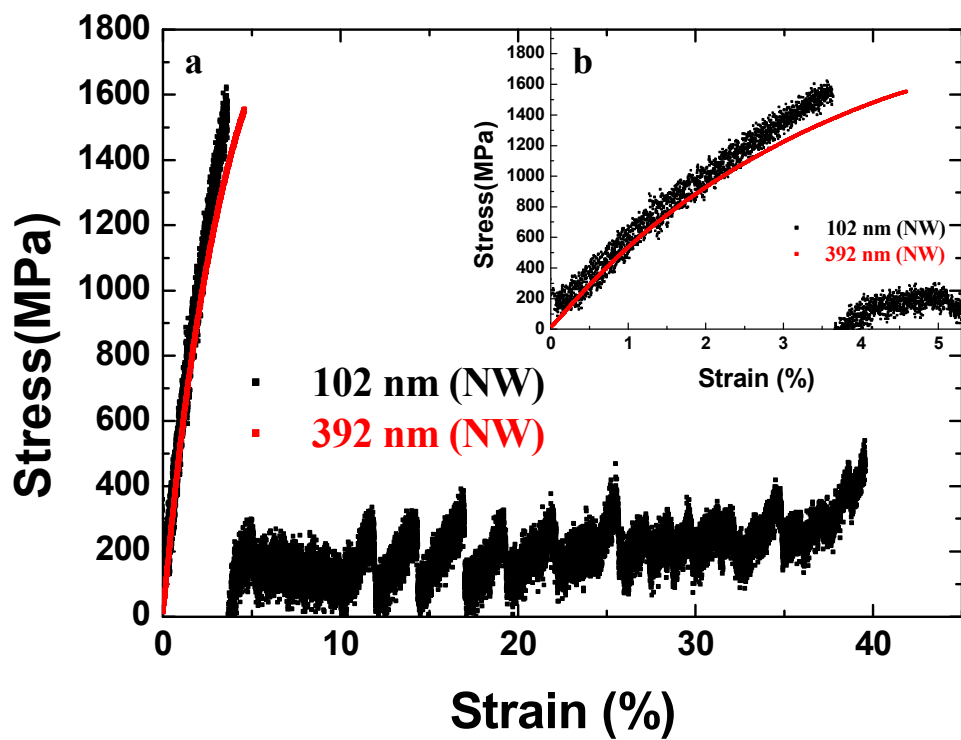
Fig. 4 Stress-strain curves of Au nanowires with diameters of 102 nm (black) and 392 nm (red)

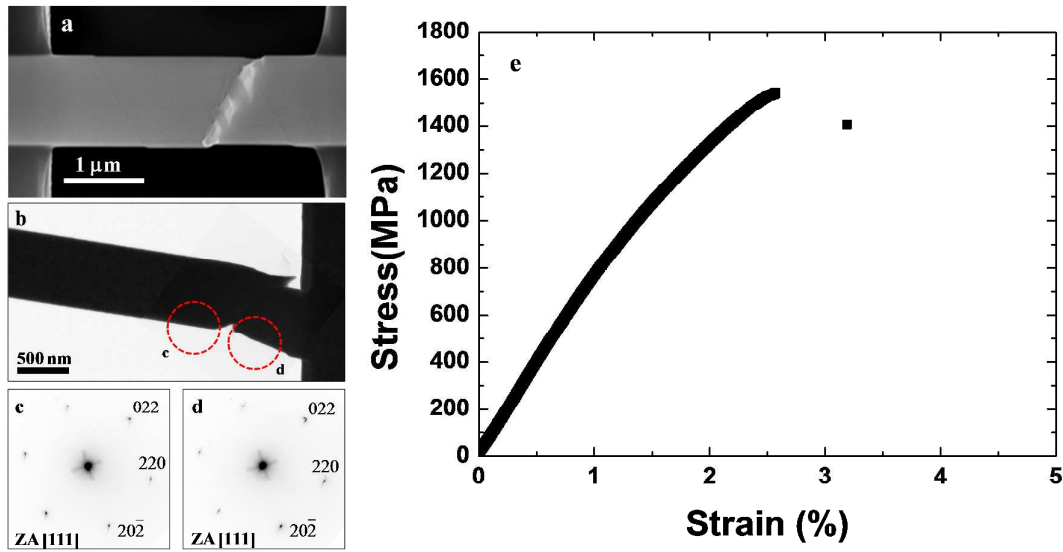up to the point of failure (a) and up to 5% strain (b).

Fig. 5 (a) A SEM image of defect-free Au nanoribbon with width-to-thickness ratio of 9:1 after failure via ordinary plasticity. (b-d) SAD patterns were taken near to deformed regions that indicated that re-orientation by twin propagation did not occur in the nanoribbon. (e) Stress-strain curve of the same nanoribbon as (a) during *in-situ* SEM tensile test.
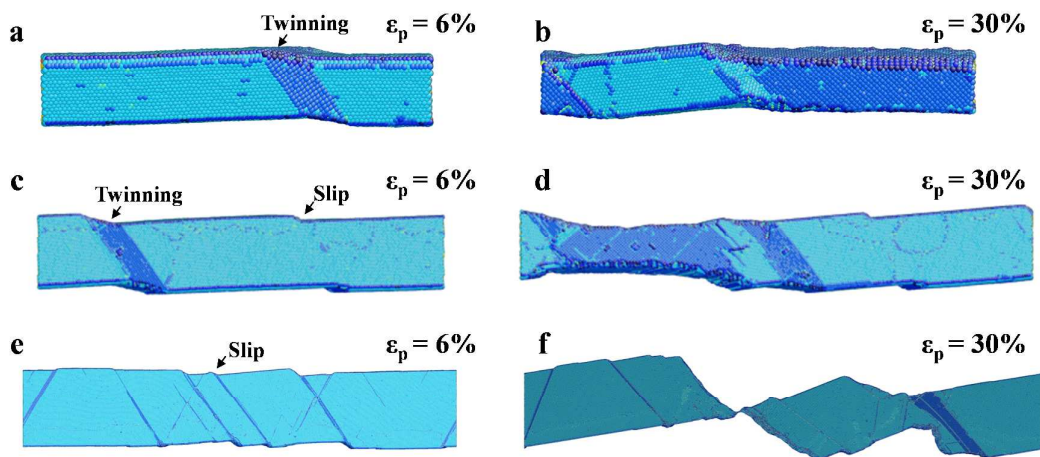
Fig. 6 Snapshots of MD simulations during tensile deformation of a typical Au nanowire that has width-to-thickness ratio of 1:1 (a, b), and Au nanoribbons that have width-to-thickness ratios of 2:1 (c, d) and 10:1 (e, f). The thicknesses of both the gold nanowire and nanoribbon were fixed to 5 nm. The Au nanowire deformed by twinning showing "superplasticity", while the Au nanoribbon deformed by full dislocation slip, and failure occurred along a slip band.